Air quality forecasts with observation-based scaling of anthropogenic emissions for urban agglomerations

Adrien Deroubaix[1,2], Guy P. Brasseur[1,3], Maria de Fatima Andrade[4], Alejandro Herman Delgado Peralta[4], Philipp Franke[5], Mario Gavidia-Calderon[4], Judith J. Hoelzemann[6], Fei Jiang[7], Inga Labuhn[8], Laurent Menut[9], Nilton Rosario[10], Guillaume Siour[11], Rita Yuri Ynoue[4],

[1]Max Planck Institute for Meteorology, Hamburg, Germany
[2]Institute of Environmental Physics, University of Bremen, Bremen, Germany
[3]National Center for Atmospheric Research, Boulder, Colorado, USA
[4]Instituto de Astronomia, Geofísica e Ciências Atmosféricas, University of São Paulo, Brazil
[5]Institute of Energy and Climate Research - Troposphere (IEK-8), Forschungszentrum Jülich GmbH, Jülich, Germany
[6]Graduate Program for Climate Sciences, University of Rio Grande do Norte, Brazil, Natal, Brazil
[7]International Institute for Earth System Science, Nanjing University, China
[8]Climate Lab, Institute of Geography, University of Bremen, Bremen, Germany
[9]Laboratoire de Météorologie Dynamique, Ecole Polytechnique, IPSL, Ecole Normale Supérieure, Université Paris-Saclay, Sorbonne Université, CNRS, Palaiseau, 91128, France
[10]Environmental Sciences Department, Federal University of São Paulo, Diadema, Brazil
[11]Univ Paris Est Creteil, Université Paris Cité, CNRS, LISA, F-94010 Créteil, France

Key Points:

- Urban air quality forecasts are improved using observation-based scaling of anthropogenic emissions
- Scaling based on observed-to-modeled concentration ratios increases forecast accuracy
- Ozone concentration forecasts are improved by volatile organic compound emission scaling while assuming a NOx-saturated chemical regime

Corresponding author: Adrien Deroubaix, `Adrien.Deroubaix@mpimet.mpg.de`

Abstract

This study presents a novel approach to improve air quality forecasts in urban agglomerations by scaling anthropogenic emissions on the basis of observed and modeled concentration ratios. Correction factors for emissions of the main primary pollutants, including NOx, SO_2, CO, $PM_{2.5}$, PM_{10}, and volatile organic compounds (VOC), are derived by comparing observed and modeled concentrations, assuming that modeled biases are primarily due to inaccuracies in anthropogenic emission inventories. The observation-based scaling approach is applied to the megacity of São Paulo, Brazil, from 6 February to 17 April 2023, demonstrating its effectiveness in refining emission magnitudes and hourly profiles within a short timeframe. We show that the approach significantly improves urban air quality forecasts for NOx, SO_2, and CO after a few weeks. In particular, O_3 concentrations are improved by correcting for VOC emissions, assuming a NOx-saturated chemical regime, which is validated by analysis of the modeled and observed chemical regimes. However, improvements for $PM_{2.5}$ and PM_{10} are limited by their links with primary trace gases that are precursors of secondary aerosols. Overall, this study demonstrates the potential of this approach to be extended to other urban agglomerations, providing valuable top-down constrains to bottom-up global anthropogenic emission inventories and improving regional air quality forecasts.

Plain Language Summary

Forecasting urban air quality is important for protecting public health, but current model forecasts are often limited by an inaccurate prescription of pollutant emissions from human activities. We developed a new approach that improves air quality forecasts by adjusting emission prescription based on observed concentrations in urban agglomerations for key pollutants such as nitrogen oxides, sulfur dioxide, carbon monoxide, particulate matter, and volatile organic compounds. Applying this new approach to the São Paulo metropolitan area, Brazilm we compared forecasted and observed pollutant concentrations (from 6 February to 17 April 2023). Using adjusted emission significantly improved air quality forecasts for São Paulo, especially for ozone levels after adjusting estimates of volatile organic compound emissions. However, the forecast of particulate matter concentrations remained challenging due to their links with gaseous pollutants. Our study demonstrates the potential of using observed concentrations in urban agglomerations to improve air quality forecasts. Extending this approach to other urban agglomerations can help refine emission estimates and improve regional air quality forecasts, enabling better decision making for health protection.

1 Introduction

Air quality forecasting in urban agglomerations is complex due to the strong diurnal evolution of pollutant emissions and concentrations in the urban boundary layer (Baklanov et al., 2016). Forecasting air quality is one of the main objectives in developing deterministic air quality chemistry and transport models to provide early warning to the population on serious air quality deterioration, particularly for O_3 and aerosols (Carmichael et al., 2008).

COVID19 has also shown that, under certain circumstances, human habits can change dramatically, leading to sudden changes in pollutant emissions and concentrations. Thanks to platforms that gather data from different air quality monitoring networks (Kosmidis et al., 2018), it becomes possible to analyze the change in atmospheric composition using near-real time observations. Using the OpenAQ data platform, Venter et al. (2020) showed that the decrease in anthropogenic emissions, mainly related to traffic, has led to an overall improvement in air quality, although O_3 concentrations have increased in several major urban agglomeration, for example in Europe (Deroubaix et al., 2021). To

accurately reproduce global changes in atmospheric composition with an air quality model (Gaubert et al., 2021), the model first requirement are updated and accurate global anthropogenic inventory as input (Doumbia et al., 2021). In addition, the air quality forecasting system based on an ensemble of models developed for China (Petersen et al., 2019; Brasseur et al., 2019) showed that during the COVID19 lockdowns only one model was able to adapt to the rapid change in emissions and predict O_3 concentrations in agreement with observations. This model uses a method for adjusting anthropogenic emissions.

Due to the large uncertainties in emission inventories, observation-based data assimilation methods have been developed in the last two decades using satellite-based observations of vertical pollutant profiles and observations from air quality monitoring networks, which have greatly contributed to improving the performance of air quality forecasts (e.g. Carmichael et al., 2008; Bocquet et al., 2015; Carrassi et al., 2018). However, the application of these methods to air quality forecasting in urban agglomerations is limited due to the coarse spatial resolution of satellite data and issues related to the spatial implementation of the monitoring network (Nguyen & Soulhac, 2021). Anthropogenic emissions in air quality models are generally provided by bottom-up emission inventories calculated by species and sector of activity (Brasseur & Jacob, 2017). The bottom-up method allows global emissions to be quantified on the basis of current knowledge of species driving processes that are not directly constrained by observed concentrations. Consequently, concentrations modeled from a bottom-up emission inventory may not be consistent with observations, which can be improved by anthropogenic emissions adjustment methods prescribed in the model. Top-down constraints derived from atmospheric observations are used to optimize emissions by applying correction factors to bottom-up emissions (Brasseur & Jacob, 2017).

The discrepancies between global and local anthropogenic emission inventories are particularly important for cities, for example in South America (Huneeus et al., 2020) and especially for vehicular emissions (Ibarra-Espinosa et al., 2020). Nowadays, there is a growing number of air quality monitoring networks implemented with low-cost sensors. Even if the accuracy of the sensors is discussed (e.g. Kumar et al., 2015; Castell et al., 2017; Wesseling et al., 2019), their rapid implementation with a large number of sensors provides satisfactory information to estimate pollutant concentrations averaged at the scale of an urban agglomeration, especially for those without a monitoring network (e.g. Kumar et al., 2015; Park et al., 2020). These local concentration observations must serve as top-down constraints on emissions to enable reliable air quality modeling in urban agglomerations where regional ensemble forecasts are not available.

This article presents a study on regional air quality forecasting with a scaling approach to impose top-down constraints on anthropogenic emissions adapted to urban agglomerations. We explain the emission scaling approach and the improvements expected for regional air quality forecasting (Section 2). Regional air quality forecasts with the anthropogenic emission scaling approach are applied to São Paulo for a period of 10 weeks in the year 2023 (from 6 February to 17 April 2023), which is comparable to the duration of an observational field campaign (Section 3). The evolution of the statistical performance of the regional forecasts is investigated for the main regulated pollutants, *i.e.* carbon monoxide (CO), nitrogen dioxide (NO_2), ozone (O_3), sulfur dioxide (SO_2), as well as $PM_{2.5}$ and PM_{10} (Section 4). Finally, development perspectives and limitations of the anthropogenic emission scaling approach are discussed (Section 5).

2 Air quality forecasts with anthropogenic emissions scaling

In this section, we explain the motivation for providing regional air quality forecasts for urban agglomerations (Section 2.1), the requirements for the monitoring net-

work (Section 2.2), the observation-based scaling approach of anthropogenic emissions (Section 2.3), and the limitations of the approach (Section 2.4).

2.1 Regional forecasts for urban agglomerations

The proposed approach to improve regional air quality forecasting is aimed at urban agglomerations that do not have an operational air quality forecasting system. In urban agglomerations, anthropogenic emission sources are dominant, and modeling errors in the concentration of short-lived primary species are mainly related to anthropogenic emissions, both in terms of magnitude and hourly profiles (e.g. Viaene et al., 2016).

Global inventories of anthropogenic emissions are often provided at a spatial resolution of 10 km (e.g. Huang et al., 2017). When they are used for global forecasts at a coarser resolution than 10 km, their information is degraded. Consequently, regional forecasts at 10 km should outperform global forecasts due to the improved spatial representation of primary pollutant emissions. Nevertheless, to provide regional forecasts with a timescale much shorter than one day, efficiency is a major constraint, requiring small horizontal modeling domains focused on urban agglomerations and configurations with chemical and aerosol models that require low computational resources. The proposed approach is dedicated to large urban agglomerations, such as megacities, where anthropogenic emissions can be assumed to be dominant.

2.2 Spatial representativeness of the observational network

To scale anthropogenic emissions, our approach consists of comparing observed and modeled concentrations and correcting emissions on the basis of this comparison. It is therefore essential to ensure that observed concentrations have a spatial representativeness consistent with the spatial resolution of the model. The number and spatial representativeness of the monitoring network's measurement stations are crucial to the proposed emission scaling approach. Internet platforms aggregating observations from different networks are providing a growing number of observations, mainly in urban agglomerations. A prerequisite for the approach is the analysis of the spatial representativeness of the monitoring network, in order to be consistent with model resolution.

2.3 Scaling of the anthropogenic emissions

The anthropogenic emission scaling approach relies on comparing observed versus modeled concentration ratios, with correction factors (CF) derived from these comparisons to adjust anthropogenic emissions for each pollutant. This approach assumes that biases between observed and modeled concentrations in urban agglomerations are primarily due to biases in anthropogenic emission inventories. Temporally, emission scaling is based on a comparison of modeled and observed concentrations averaged over the last few days. Averaging only the last week allows rapid variations in emissions to be captured, for example during events such as COVID-19 or other special events. A time scale of less than a week mixes weekdays and weekends, and is therefore inconsistent. Spatially, emission scaling can be carried out locally around a station, for a limited spatial area, or for an entire urban agglomeration if anthropogenic emissions can be considered uniform.

The approach consists of two complementary emission scaling calculations, based on daily or hourly concentrations averaged over the last week. CF are calculated weekly for NOx, SO_2, CO, $PM_{2.5}$ and PM_{10} to provide daily or hourly emission-scaled forecasts. For VOC, CF are determined based on modeled O_3 biases, assuming a NOx-saturated regime. Three regional forecasts are initiated daily, each differing in their anthropogenic emissions:

- F-REF (reference forecast),
- F-DAY (daily emission-scaled forecast),
- F-HOUR (hourly emission-scaled forecast).

2.3.1 Correction factors of NOx, SO_2, CO, $PM_{2.5}$ and PM_{10}

Correction factors (CF) are calculated for NOx, SO_2, CO, $PM_{2.5}$ and PM_{10}.

(i) With the daily emission-scaled forecast, a single CF-daily is calculated based on the ratio of the observed and modeled weekly concentration averages (WCA):

$$CF - daily(w) = \frac{WCA_{obs}(w-1)}{WCA_{mod}(w-1)} \tag{1}$$

Where w represents a given week.

(ii) With the hourly emission-scaled forecast, 24 CF-hourly are calculated based on the ratio of the observed and modeled weekly concentration averages per hour (WCAH):

$$CF - hourly(w,h) = \frac{WCAHobs(w-1,h)}{WCAHmod(w-1,h)} \tag{2}$$

Where h represents a given hour.

2.3.2 Correction factor of VOC

There are no routine observations of VOC concentrations due to the difficulty in measuring their various components, so information about VOC comes primarily from observational field campaigns (Theloke & Friedrich, 2007). As a result, VOC emissions from global anthropogenic inventories may not accurately reflect the reality of most megacities (Sokhi et al., 2022). Consequently, we propose to determine VOC-CF based on modeled O_3 biases.

O_3 is a secondary pollutant formed during the day, depending on the relative amounts of VOC and NOx (e.g. Monks et al., 2015). Assuming a NOx-saturated regime, the production of O_3 is controlled by the VOC concentration. Therefore, if the modeled O_3 concentration is overestimated, it implies an overestimation in VOC, and conversely for an underestimation. Based on this assumption, a single CF is calculated for VOC emissions based on the ratio of the observed and modeled maximum O_3 concentration (MaxO3) of the hourly average diurnal cycle of the previous week:

$$CF - daily(w) = \frac{MaxO3_{obs}(w-1)}{MaxO3_{mod}(w-1)} \tag{3}$$

As NOx-CF differs for F-DAY and F-HOUR, the modeled O_3 concentrations are expected to be different, resulting in different VOC-CF.

After several weeks, the evolution of the correction factors for both daily and hourly approaches, along with their impact on statistical performance, is analyzed. This information is then interpreted to adjust the inventory of anthropogenic emissions used for the regional forecasts in terms of magnitude and hourly profiles.

2.4 Limitations of observation-based emission scaling

- NOx

For NOx, composed of NO and NO_2, the emissions scaling approach should be effective due to their short lifetimes. However, their links with O_3 chemistry lead to high

diurnal variability in NOx concentrations. Moreover, the spatial representativeness of the monitoring network could lead to inaccurate CF, especially for NO.

- SO_2

The SO_2 emission scaling approach is also expected to be efficient due to its short lifetime, although conversion to sulfate may affect modeled $PM_{2.5}$ and PM_{10} concentrations.

- CO

The CO emission scaling approach may be less efficient due to its longer lifetime (much longer than NOx and SO_2), which could results in a large influence of CO transported from outside the urban agglomeration.

- $PM_{2.5}$ and PM_{10}

$PM_{2.5}$ and PM_{10} are composed of carbonaceous, inorganic, mineral, and marine aerosols, which vary widely in urban agglomerations (e.g. Cheng et al., 2016). In addition, secondary organic and inorganic aerosols are formed in the atmosphere depending on the amount of gaseous precursors and meteorological conditions (e.g. Zhang et al., 2009). For aerosols (*i.e.* $PM_{2.5}$ and PM_{10}), the emission scaling approach is expected to be limited because of the complexity of their composition and relationships with gaseous precursors, and because of the transport of aerosols from outside the agglomeration.

- VOC

To correct VOC emissions, an additional assumption is necessary regarding the chemical regime, which must be NOx-saturated for the VOC-CF to be efficient. Therefore, it is essential to verify this assumption, which can be achieved through indicators of the chemical regime (Liang et al., 2006). These indicators are concentration ratios of chemical species associated with the formation of tropospheric O_3 through cycling chain reactions involving OH, HO_2, and RO_2 (Levy, 1971). Zhang et al. (2009) discuss the robustness of these indicators and demonstrate their consistency when the chemical regime is well established. Among the different indicators, only O_3 / NOx can be studied for both observations and forecasted concentrations. A NOx-saturated regime is well defined by the O_3 / NOx indicator when the value is below 15 (Zhang et al., 2009). The VOC emission scaling approach may enable the modeled chemical regime to be more consistent with the observations.

3 Regional forecasts for São Paulo, Brazil

3.1 Methodology applied to São Paulo

The regional forecasts were initiated on 30 January 2023, and the assessment covers the period from 6 February to 17 April 2023. This period includes the São Paulo Carnival (11-19 February), which may have an impact on anthropogenic emissions.

The choice to focus on São Paulo has been motivated by several factors: (i) its status as South America's largest megacity, lacking a regional air quality forecast, (ii) the presence of a high-quality monitoring network (Andrade et al., 2017), (iii) the variability of the megacity's air quality due to high anthropogenic emissions, and (iv) modeled air quality in São Paulo has been investigated by a model intercomparison (Deroubaix et al., 2024).

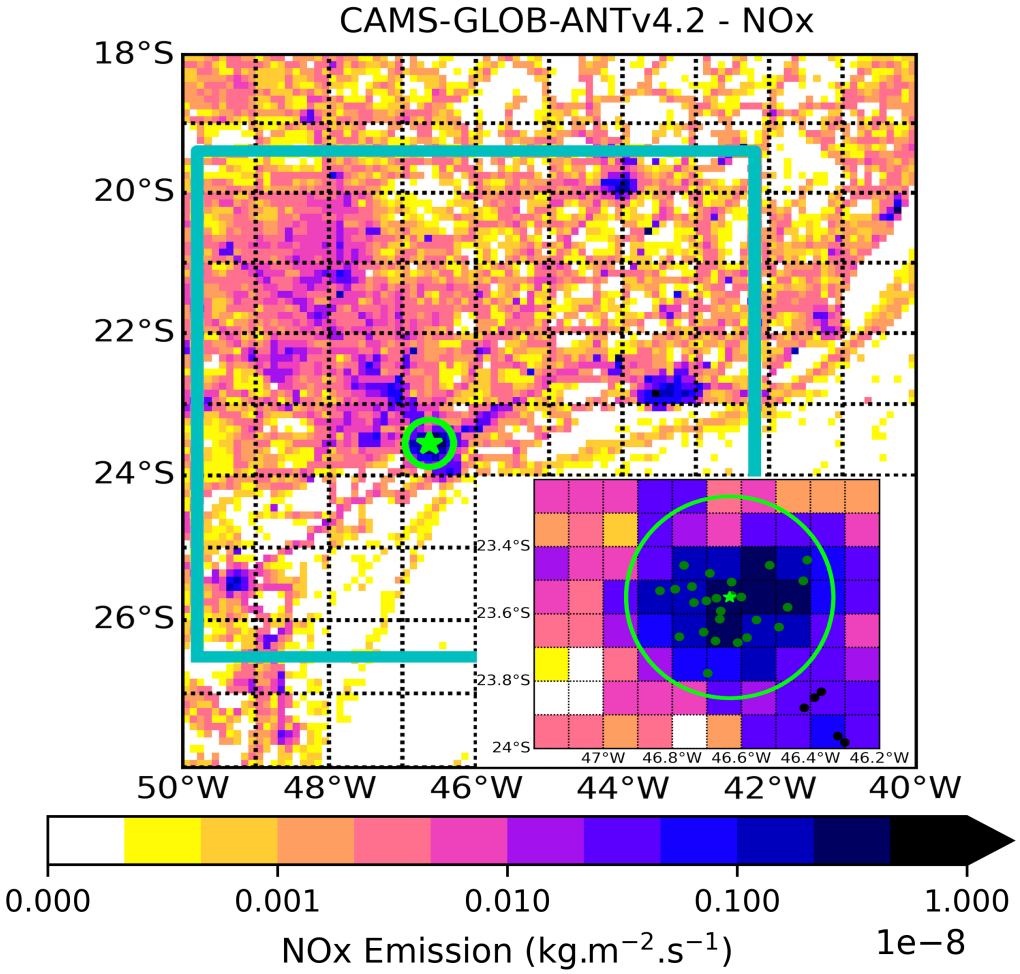

Figure 1. *NOx emission flux maps (sum of all sectors) for the São Paulo region from the CAMS-GLOB-ANTv4.2 anthropogenic inventory, with a zoom on the most densely populated area of the megacity (inside the green circle). The horizontal modeling domain used for regional forecasts corresponds to the blue rectangle. On the zoom (bottom right), the locations of the air quality monitoring network stations (dots) are shown, with the distinction of the 26 stations within the most densely populated area of the megacity (inside the green circle). São Paulo's traditional city center is located at the Catedral da Sé (green star), which is used as the center of the 30-km radius circle.*

The horizontal modeling domain covers areas with high anthropogenic emissions, and it includes a significant portion of the ocean in order to reproduce the land-sea breeze, which play an important role in the pollutant transport and removal (Freitas et al., 2007). NOx annual emission fluxes are depicted for the São Paulo region, along with the locations of the measurement stations (Figure 1). The monitoring network comprises 26 stations within a 30-km radius circle centered at São Paulo's traditional city center (Catedral da Sé), ensuring adequate coverage of high NOx anthropogenic emission areas, reaching up to 2.3×10^{-9} kg.m^{-2}.s^{-1}.

3.2 Configuration of the daily regional forecasts

The regional forecasts use the WRFchem model (Grell et al., 2005; Fast et al., 2006; Powers et al., 2017) combined with the WACCM6 (hereafter WACCM) forecast (Gettelman et al., 2019) provided by NCAR (Table A1). The daily updated datasets include, for meteorology the FNL dataset from the US National Centers for Environmental Prediction (NCEP, 2023), for fire emissions the FINNv1 dataset (Wiedinmyer et al., 2011) and for chemical boundary conditions the WACCM forecasts (Gettelman et al., 2019). Five steps are performed daily to produce the regional forecasts: (1) preprocessing of NCEP meteorological data, (2) calculation of fire, biogenic, and anthropogenic emissions, (3) integration of WACCM forecasts as chemical boundary conditions, (4) simulation of air quality for the next two days with WRFchem, (5) interpolation of the forecasts at the city center and comparison with air quality station data.

The modeling domain consists of a small horizontal grid of 80 x 80 cells with 37 vertical levels, which gives importance to the meteorological and chemical boundary conditions (Table A1). The model configuration is close to that used by Deroubaix et al. (2024), but the domain spatial resolution is reduced and without nested domain. The resolution is 10 km, corresponding to the resolution of the anthropogenic emissions inventory (Granier et al., 2019), with sectoral hourly profiles (Crippa et al., 2020), which differ depending on weekdays (Figure A1). The chemical scheme is MOZART4 (Emmons et al., 2010), and the aerosol scheme is GOCART (Chin et al., 2002), ensuring fast forecast computation (Pfister et al., 2011). With this setup, the air quality forecast for the next two days can be produced in about 2 hours using 40 processors. About 7 GB of data are stored per day, which amounts to about 2.5 TB per year.

3.3 Spatial representativeness of the monitoring network

Observations are obtained from the OpenAQ data platform via an API (Application Protocol Interface), which allows fast and portable data access (OPENAQ, 2023). In order to derive the correction factors (CF) of anthropogenic emissions, a super-observation of pollutant concentration in the city center is calculated from the measurement stations of the São Paulo monitoring network for each pollutant. Different calculations of the super-observation are possible to derive CF and to modify anthropogenic emissions (*cf.* Section 2.2). The methodology of Deroubaix et al. (2024) is adapted to the location of the stations in the São Paulo monitoring network in order to ensure the spatial representativeness of the super-observation corresponding to the entire megacity. The super-observation used in this study is based on the measurement stations within a 30-km radius of the city center (Figure 1). Using inverse distance weighting interpolation, the city super-observation is calculated and compared to the forecasted concentrations interpolated at the city center. From these comparisons, CF are derived for each pollutant. These CF, calculated on Monday, are applied to anthropogenic emissions for the rest of the week. For NOx, the CF are based only on the NO_2 concentration due to sparse NO data and its short lifetime.

4 Forecast performance evaluation for São Paulo

The regional forecasts are evaluated for São Paulo for a 10-week period (6 February to 17 April 2023). The scaling of anthropogenic emissions is done on Mondays (*i.e.* the CF-daily and CF-hourly calculations). Thus, this section analyzes the evolution of the statistical performance from one week to the next, for NOx (Section 4.1), for SO_2, CO, $PM_{2.5}$ and PM_{10} (Section 4.2), and for VOC (Section 4.3).

First, the week-to-week evolution of the correction factors (CF) is studied during the 10-week period in order to determine if the CF converge to a value after some weeks. Second, the weekly evolutions of the statistical performance of the three regional forecasts are investigated for each pollutant using two statistical metrics (1) the model biases and (2) the root mean square error (RMSE). The difference in performance for the next day (d+1) and the day after (d+2) is also evaluated with the same statistical metrics, and compared to two global forecasts, the WACCM forecast (Gettelman et al., 2019) with a spatial resolution of about 100 km and the CAMS forecast (ECMWF, 2023) with a finer resolution of about 40 km (Table A1).

4.1 NOx emission scaling evaluation

We first focus on NO_2, for which we expect the emission scaling approach to be efficient due to the short lifetime of NO_2. Moreover, we choose to scale NOx emission using the CF calculated on NO_2, thus NO_2-CF are equivalent to NOx-CF. The NO_2-CF used for the scaling of daily and hourly emissions are presented over the 10-week period (Figure 2-a).

With the daily emission scaling, NOx emissions are reduced by half in the first week. The CF value is ≈ 0.5, and then this value varies slightly until the end of the period. With the hourly emission scaling, CF tends to decrease emissions during the night but increasing emissions during the day, leading to modifications of the hourly emission profile. The mean of hourly NO_2-CF tend to be higher (≈ 0.8) than daily NO_2-CF (Figure A2).

From the first week evaluated (6 to 13 February), modeled NO_2 biases are reduced for both emission-scaled forecasts (Figure 2-b). The evolution of the statistical performance over the 10 weeks shows that both emission-scaled forecasts lead to a strong reduction in weekly NO_2 biases of ≈ 20 ppb compared to the reference. In addition, the RMSE is also reduced by ≈ 10 ppb compared to the reference (Figure A2). The forecasts produced for d+1 and for d+2 are similar in terms of bias and RMSE for all forecasts. The daily and hourly emission-scaled forecasts lead to lower biases and RMSE than the two global forecasts and the reference (Figure A2).

Both regional emission-scaled forecasts are based on modeled biases averaged over the last week. The average hourly diurnal cycles are examined because the emission-scaled forecasts are expected to be in better agreement with observations than the reference forecast (F-REF) from the first week evaluated (Figure 3).

The modeled NO_2 concentration is underestimated during the day and overestimated during the night for both F-DAY and F-REF. Although the biases for daily emission-scaled forecast (F-DAY) are increased during the day compared to the reference forecast (F-REF), the diurnal cycle of the modeled NO_2 is improved in magnitude as there is a strong reduction in biases of up to 20 ppb during the night. With the hourly emission-scaled forecast (F-HOUR), the hourly mean diurnal cycle is improved for each hour compared to F-REF. There is a large reduction in bias during the night (up to 25 ppb) compared to F-REF, which is a negligible bias during the day. Consequently, this scaling, which modifies the hourly emission profile, leads to the best agreement with observations. Nevertheless, there is an overestimation of NO_2 concentrations in the morning at 09:00 and in the evening at 18:00, two hours later than the traffic emission peaks at 07:00 in

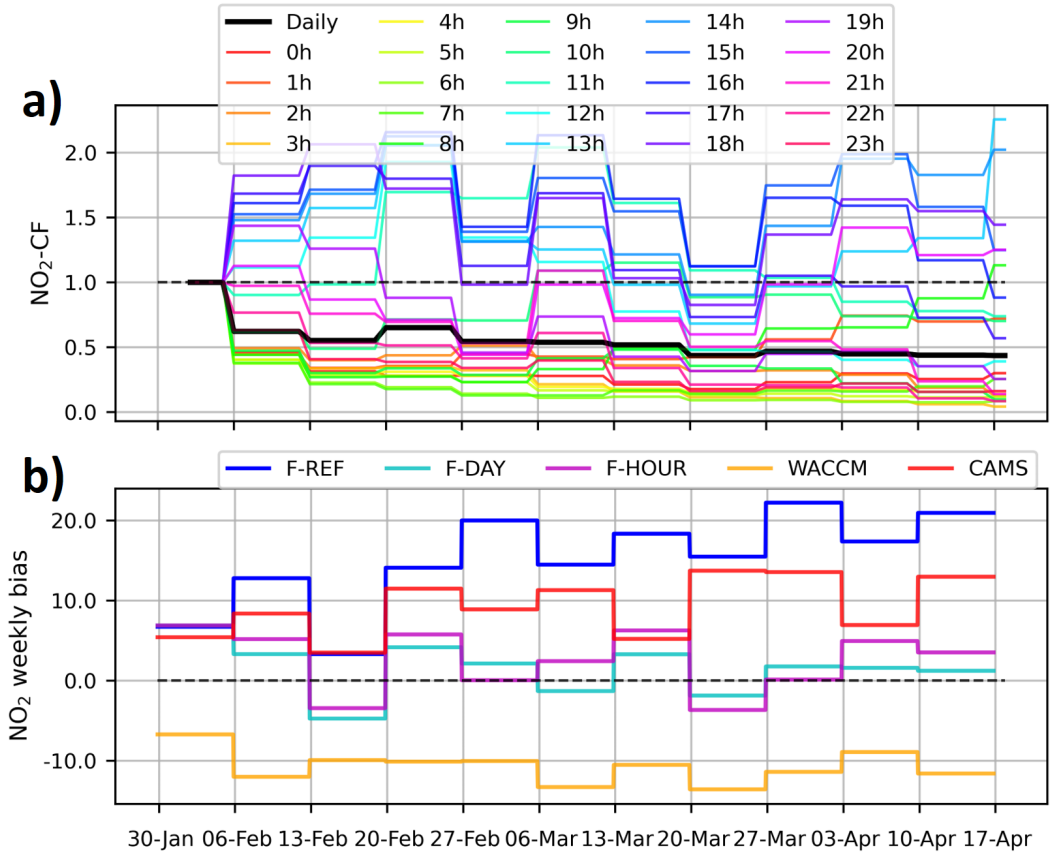

Figure 2. *Weekly evolution of (a) daily and hourly NO_2 correction factors (CF) used for the daily and hourly emission-scaled forecasts (F-DAY and F-HOUR) of a given week, and (b) mean bias of NO_2 forecasted concentrations (in ppb), for the three regional forecasts (F-REF, F-DAY and F-HOUR), and for the two global forecasts: (iv) WACCM provided by NCAR and (v) CAMS provided by ECMWF, over the 10-week period (in 2023) in the center of São Paulo. Hours are given in local time (GMT-3).*

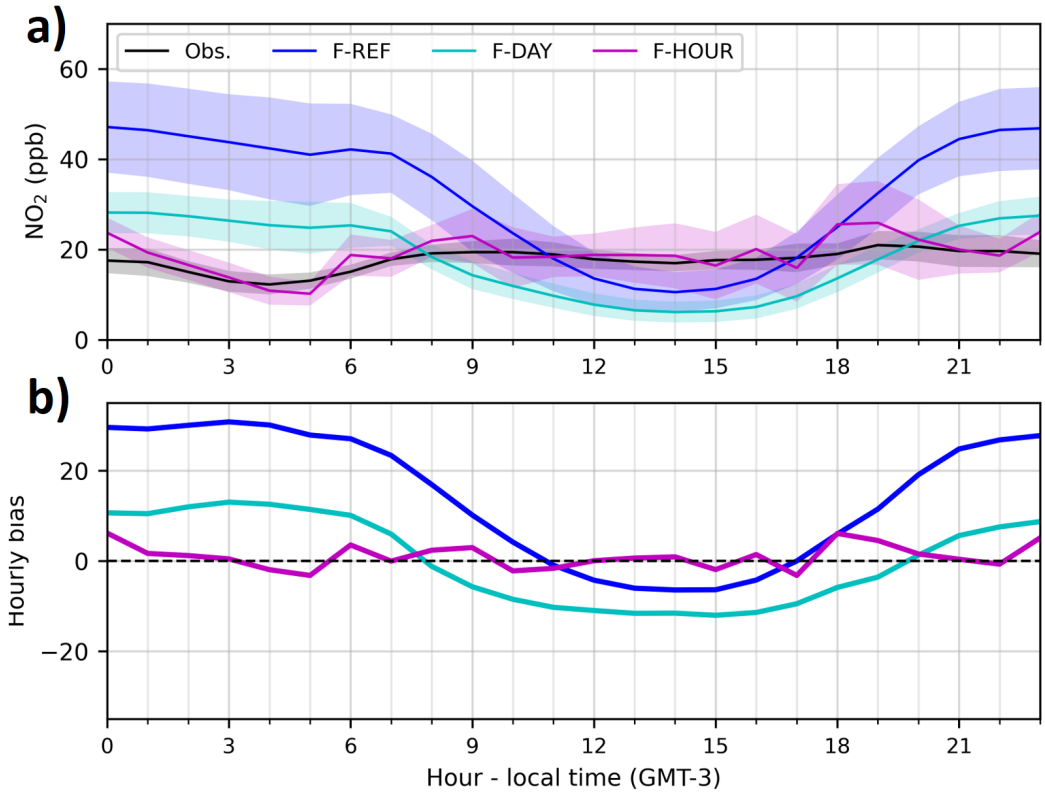

Figure 3. *(a) Average hourly diurnal cycles of observed and forecasted NO_2 concentrations from the second week to the end of the 10-week period (13 February to 17 April 2023) in the center of São Paulo. Modeled concentrations correspond to the three regional forecasts: (i) F-REF, the reference forecast, (ii) F-HOUR, the hourly emission-scaled forecast, and (iii) F-DAY, the daily emission-scaled forecast. The color shades correspond to the standard deviation of the concentrations for each hour of the period. (b) Average hourly biases of the three regional forecasts, which are the differences in the average hourly diurnal cycles of observed and modeled NO_2 concentrations (shown in panel a).*

the morning and 16:00 in the evening prescribed in the model (Figure A1). The CF of these hours do not tend to converge after 10 weeks, while the CF of the other hours tend to a clear value (Figure 2-a). This result suggests that the hourly emission scaling compensates for biases that are not solely related to the hourly profiles of anthropogenic emissions, such as a poor representation of the height of the urban boundary layer, which changes rapidly in the morning and evening, and which could be related to the absence of the urban heat island effect in the model, leading to an underestimated height (Deroubaix et al., 2024).

Although the approach is limited by the allocation to different sectors in the anthropogenic emission inventories, the CF tend to 0.5 for the daily emission-scaled forecast and 0.8 for the hourly one, so the NOx anthropogenic emissions from the used inventory should be reduced in São Paulo. This reduction of the emission in the center of São Paulo is in agreement with the previous study of Vivanco and de Fatima Andrade (2008). In addition, hourly CF increase during the day and decrease at night, so hourly emission profiles should be modified accordingly, but the CF obtained for morning and evening should be taken with caution. In conclusion, regional forecasts with the emission scaling approach reduce the mean weekly NO_2 bias, and the reduction is similar for the daily and hourly emission-scaled forecasts. However, only the hourly emission-scaled forecast leads to a better representation of the average hourly diurnal NO_2 cycles, suggesting that the hourly emissions profiles could be revised using hourly CF information.

4.2 SO_2, CO, $PM_{2.5}$ and PM_{10} emission scaling evaluations

Deroubaix et al. (2024) have shown that SO_2 concentration is largely overestimated by air quality models in central São Paulo in 2019. For both emission-scaled forecasts, SO_2-CF are reduced from the first week and then tend towards a value of ≈ 0.1 (Figure 4-a). Except for the 05:00 correction factor, we note that the SO_2-CF increases from the third week to the end of the period, reaching a value of 4. This result reflects a problem with the calibration of the measuring instruments, which were all carried out at the same time, except for one station close to the SO_2 sources. The bias therefore changes during this hour, due to the problem of spatial representativeness of this station for the megacity.

The evolution of weekly mean SO_2 biases for the three regional simulations and the two global forecasts shows that the reference simulation has the largest bias (Figure 4-b). The CAMS and WACCM forecasts have biases of ≈ 5 ppb, while F-REF reaches 20 ppb. Both F-DAY and F-HOUR significantly reduce biases, which tend towards 0 at the end of the period. In addition, the mean bias and RMSE of SO_2 are reduced in the same proportions for d+1 and for d+2 (Figure A3). Consequently, with emission scaling approach, regional forecasts of SO_2 are in good agreement with observations in terms of temporal variability.

Compared to NO_2 and SO_2, CO has a longer lifetime, so the influence of emission sources outside São Paulo, which are not affected by the anthropogenic emission scaling, is stronger. The daily emission-scaled forecast for CO leads to a CF with a value of ≈ 0.5 from the first week to the end of the period (Figure 4-c), which is also the case for the mean hourly CO-CF (Figure A4). With the hourly emission-scaled forecast, CO-CF associated with the hours from 11:00 to 05:00 are reduced beyond the value obtained with the daily CF, while for the other hours, CO-CF are increased. CF are even higher than 1 in the morning and evening for hours associated with peak traffic emissions. Over the 10-week period, the F-REF and CAMS overestimate CO by ≈ 0.1 ppm, while WACCM underestimates CO by ≈ 0.2 ppm (Figure 4-d). Both F-DAY and F-HOUR lead to small biases from the fourth week of the period onwards. For both forecasts, the RMSE is reduced by ≈ 0.1 ppm compared with F-REF for d+1 and also for d+2. As a result, the temporal variability of CO concentration is improved with the emission scaling approach

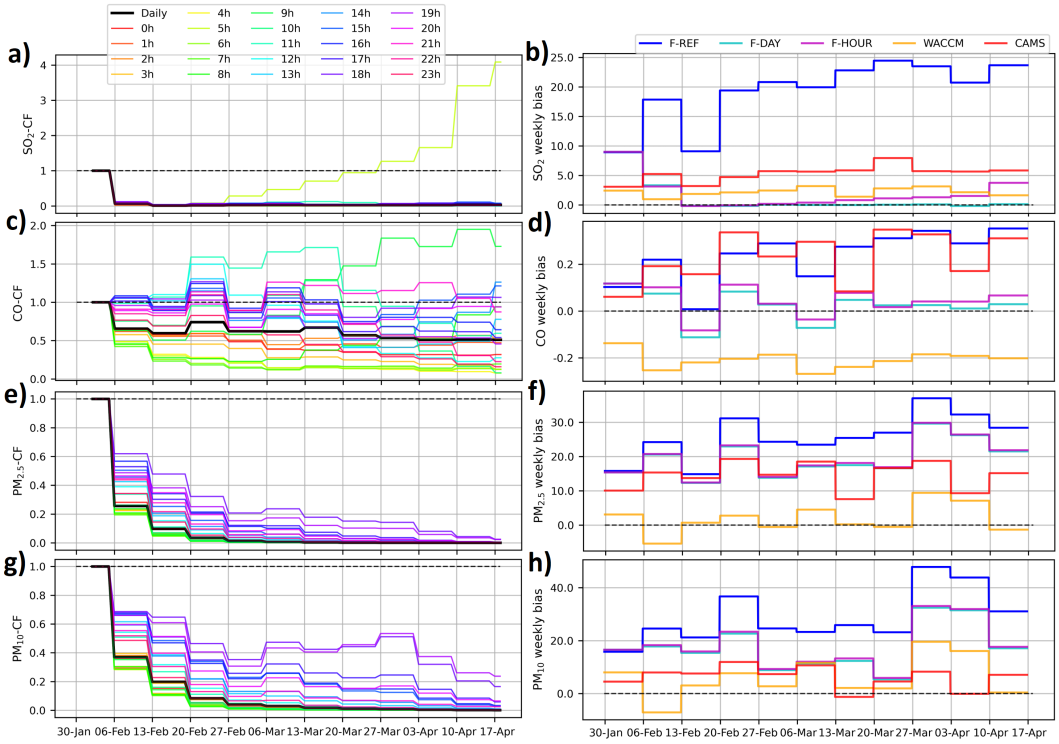

Figure 4. *Weekly evolution of (a, c, e and g) daily and hourly correction factors (CF) for CO, SO_2, $PM_{2.5}$ and PM_{10} used for the daily and hourly emission-scaled forecasts (F-DAY and F-HOUR) of a given week, and (b, d, f and h) mean biases of forecasted concentrations of SO_2 (in ppb), CO (in ppm), $PM_{2.5}$ and PM_{10} (in $\mu g.m^{-3}$), for the three regional forecasts (F-REF, F-DAY and F-HOUR), and for the two global forecasts: (iv) WACCM provided by NCAR and (v) CAMS provided by ECMWF, over the 10-week period (in 2023) in the center of São Paulo. Hours are given in local time (GMT-3).*

in center of São Paulo. However, the RMSE is greater than 0.1 ppm for all forecasts, suggesting that some emission sources are missing or their intensities are inaccurate (Figure A4).

Investigating the PM forecasts, the anthropogenic emissions are largely reduced after three weeks, as CF tend towards a very low value below 0.2 for both emission-scaled forecasts from week 4 to the end of the period (Figure 4-e and g). This leads to the strong reduction of anthropogenic PM emissions in the center of the megacity from week 4 onwards. Weekly PM biases are reduced with the same intensity for both F-DAY and F-HOUR from week 4 onwards (Figure 4-f and h). Thereafter, there is no significant change in mean bias. Compared with the F-REF, the biases for $PM_{2.5}$ are reduced by ≈ 5 µg.m^{-3} and by ≈ 10 µg.m^{-3} for PM_{10}. CAMS overestimates $PM_{2.5}$ by ≈ 10 µg.m^{-3}, while for PM_{10} the bias is less than ≈ 5 µg.m^{-3}. The two global forecasts have the lowest biases and RMSE for $PM_{2.5}$ and PM_{10}. In addition, the three regional forecasts have lower statistical performances than the two global forecasts, with no difference between d+1 and d+2 (Figures A5 and A6).

Although PM-CF is very low and therefore anthropogenic emissions are largely reduced, model biases remain positive. This overestimation of PM suggests that the model overestimates the proportion of PM transported from outside the center of São Paulo. Considering the hourly emission-scaled forecast, PM-CF for evening hours are higher than those for other hours, showing that model biases are lower than during the rest of the day, suggesting that anthropogenic PM contributes significantly to total evening PM. Furthermore, if we compare $PM_{2.5}$ and PM_{10}, we find that the correction factor for $PM_{2.5}$ is stronger during the day (≈ 0.1) than that for PM_{10} (≈ 0.2), which may be linked to an overestimation of secondary aerosol production.

4.3 VOC emission scaling evaluation

For São Paulo, Deroubaix et al. (2024) have shown that a regional simulation using a local anthropogenic inventory and without biogenic emissions reproduces the O_3 concentration in good agreement with observations, challenging the values of global anthropogenic inventories that have significant VOC emissions in the center of the megacity. Using the emission scaling approach for VOC under the assumption that the regime is saturated with NOx (*i.e.* controlled by the VOC concentration), the bias of the maximum daily O_3 concentration should be reduced as the approaches modify the chemical regime compared to the reference forecast, which depends on the NOx / VOC ratio.

VOC-CF are largely reduced from the first week for both F-DAY and F-HOUR, and tend to be less than 0.1 from the sixth week onwards (Figure 5-a). This result indicates that the modeled daily maximum of O_3 is overestimated during the first five weeks of the period for both emission-scale forecasts. As NOx-CF are different for the two emission-scaled forecasts , this leads to different changes in the ratio between NOx-CF and VOC-CF (*cf.* Section 2.3). The change in NOx emissions is greater with the daily CF (NOx-CF ≈ 0.5) than with the hourly CF (NOx-CF ≈ 0.8). As a result, the NOx-CF / VOC-CF ratios increase over the 10-week period, reaching a value of ≈ 30 for the hourly CF and ≈ 120 for the daily CF. Therefore, NOx emissions decrease much less than VOC emissions for both emission-scale forecasts. This analysis of the evolution of VOC-CF versus NOx-CF supports the assumption of a NOx-saturated regime in center of São Paulo.

To verify the assumption of a NOx-saturated regime, the O_3 / NOx ratio is studied for both observations and regional forecasts (Figure 5-b). A value of this ratio of less than 15 is associated with a NOx-saturated regime (Zhang et al., 2009). The scaling of VOC emissions does not result in a modeled O_3 / NOx ratio for F-DAY and F-HOUR that is more consistent with the observed variability than F-REF. However, the observed and modeled values are clearly associated with a NOx-saturated regime, confirming that the assumption is appropriate for São Paulo (over the period studied).

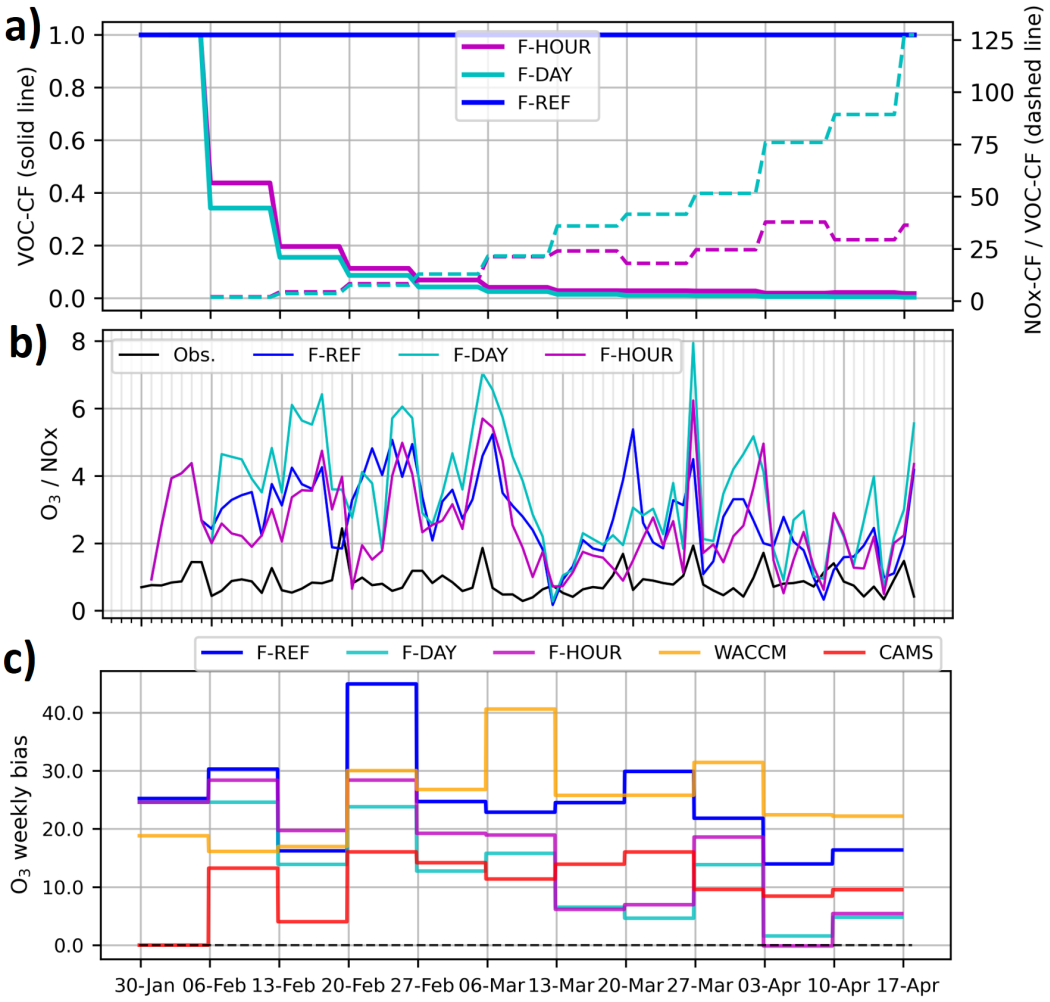

Figure 5. *Weekly evolution of (a) VOC correction factors (CF) used for the daily and hourly emission-scaled forecasts (F-DAY and F-HOUR) of a given week together with the NOx-CF / VOC-CF ratio, (b) O_3 / NOx ratio for the observation and the three regional forecasts (F-REF, F-DAY and F-HOUR), and (c) mean biases of O_3 forecasted concentrations, for the three regional forecasts (F-REF, F-DAY and F-HOUR), and for the two global forecasts: (iv) WACCM provided by NCAR and (v) CAMS provided by ECMWF, over the 10-week period (in 2023) in the center of São Paulo.*

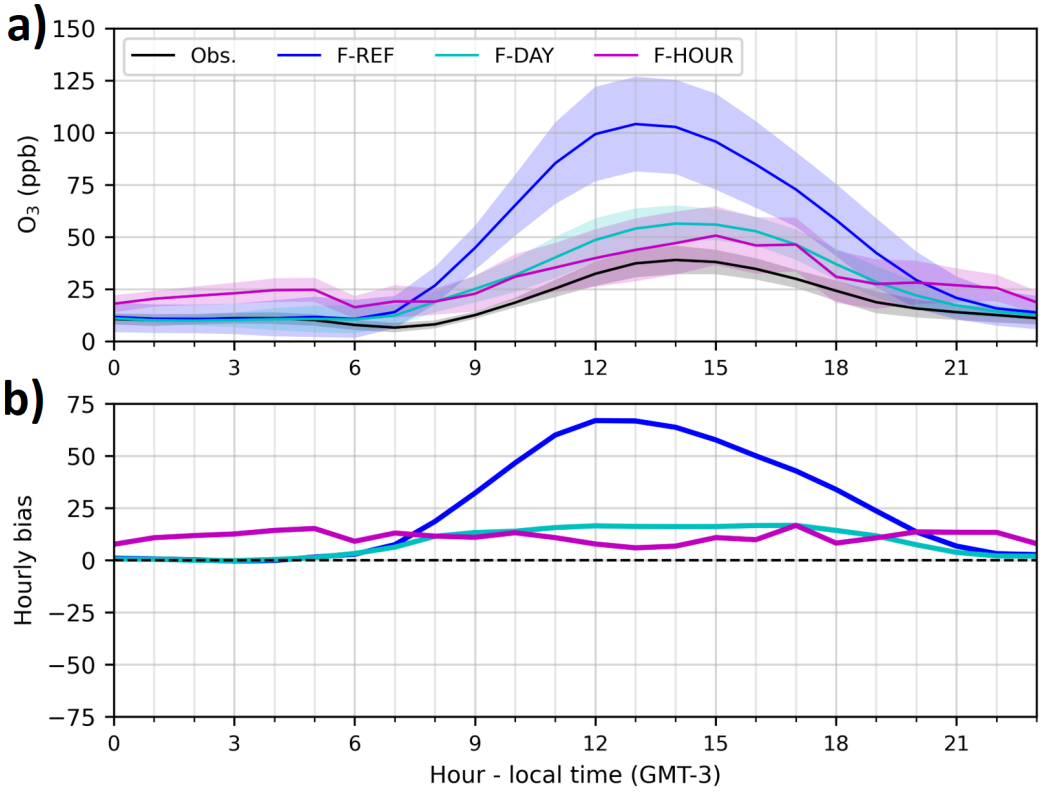

Figure 6. *(a) Average hourly diurnal cycles of observed and modeled O_3 concentrations from the sixth week to the end of the 10-week period (13 March to 17 April 2023) in the center of São Paulo. Modeled concentrations correspond to the three regional forecasts: (i) F-REF, the reference forecast, (ii) F-HOUR, the hourly emission-scaled forecast, and (iii) F-DAY, the daily emission-scaled forecast. The color shades correspond to the standard deviation of the concentrations for each hour of the period. (b) Average hourly biases of the three regional forecasts, which are the differences in the average hourly diurnal cycles of observed and modeled O_3 concentrations (shown in panel a).*

Over the 10-week period, the statistical performance for O_3 of F-REF is lower than the CAMS global forecast and comparable to the WACCM forecast both in terms of mean weekly bias (Figure 5-c) and RMSE (Figure A7). For both emission-scaled forecasts, a significant reduction in mean weekly bias and RMSE is observed after five weeks, whereas the reduction in NOx-CF is reached after two weeks (*cf.* Section 4.1). From the sixth week of the period onwards, F-DAY and F-HOUR have the best statistical performance for O_3 for the next day (d+1) and the day after (d+2), both in terms of mean weekly bias (Figure 5-c) and RMSE (Figure A7).

We examine the changes in average hourly diurnal cycles obtained between the sixth week and the end of the 10-week period. F-REF overestimates O_3 concentrations during the day (06:00 to 21:00), while the daytime O_3 bias is reduced by more than 25 ppb for both emission-scaled forecasts. The best agreement is obtained with F-DAY, because F-HOUR leads to an overestimation of O_3 concentrations at night. These results suggest that not only the magnitude of anthropogenic emissions and hourly profiles need to be revised, but also that the reduction in NOx emissions at night is too strong for F-HOUR, which again points to an underestimation of the urban boundary layer height at night due to the absence of the urban heat island effect in the model.

5 Conclusions

In this study, we present a new approach to improve air quality forecasts in urban agglomerations using observation-based scaling of anthropogenic emissions. The proposed approach assumes that in large urban agglomerations, such as megacities, biases between observed and modeled concentrations arise mainly from biases in anthropogenic emissions. The approach consists in deriving daily and hourly correction factors for NOx, SO_2, CO, $PM_{2.5}$ and PM_{10} based on the comparison of observed and modeled concentration ratios using daily and hourly averages respectively. For VOC, the emission scaling is determined on the basis of modeled O_3 biases during the day, assuming a NOx-saturated regime.

The implementation of the approach in São Paulo shows that a substantial reduction of anthropogenic NOx emissions is required. The hourly emission-scaled forecast significantly improves NO_2 concentration forecasts compared to the daily emission-scaled forecast, indicating that both the magnitude and hourly emission profile can be refined using information obtained over a 10-week period. In addition, ozone concentrations are improved over the study period by correcting for VOC emissions, with adjustments made under the validated assumption of a NOx-saturated chemical regime in the center of São Paulo. The approach also performs well for SO_2 and CO, while improvements for PM are limited due to the transport of biomass burning aerosols and secondary aerosol formation.

The implementation of this approach for regional forecasts (or the analysis of a past period) provides valuable insights within a short timeframe and informs further needed adjustments to anthropogenic emission magnitudes and temporal emission profiles. However, the accuracy of the observation-based emission scaling is limited by four key factors: (i) the modeling of the urban meteorology, (ii) the spatial representativeness of the monitoring network, (iii) the transport of pollutants from outside the urban agglomeration, and (iv) the links between primary trace gases that are precursors of secondary organic or inorganic aerosols.

In conclusion, the proposed approach to improve regional forecasts can be tested and implemented in other urban areas. For a specific urban agglomeration, the approach provides valuable top-down constrains to bottom-up global anthropogenic emission inventories and improves regional air quality forecasts.

Open Research Section

Availability of the data: The observed and forecasted pollutant concentrations analyzed in this study are available through this web link: `https://zenodo.org/records/10977856`, last access: April 16, 2024 [Dataset].

Acknowledgments

AD acknowledges the European Union's Horizon 2020 research and innovation programme for supporting this work under the Marie Skłodowska-Curie grant agreement No 895803 (MACSECH — H2020-MSCA-IF-2019).

This article is a direct contribution to the research themes of the Klimapolis Laboratory (klimapolis.net), which is funded by the German Federal Ministry of Education and Research (BMBF).

GB acknowledges the National Center for Atmospheric Research, which is sponsored by the US National Science Foundation.

// Authors contribution:

AD designed the study, performed the analysis and wrote the first draft. All authors contributed to the final version of the manuscript.

The authors gratefully acknowledge the resources of the Deutsches Klimarechenzentrum (DKRZ) granted by its Scientific Steering Committee (WLA) under project ID bm1257.

References

Andrade, M. d. F., Kumar, P., de Freitas, E. D., Ynoue, R. Y., Martins, J., Martins, L. D., ... Zhang, Y. (2017, 6). Air quality in the megacity of são paulo: Evolution over the last 30 years and future perspectives. *Atmospheric Environment*, *159*, 66-82. doi: 10.1016/j.atmosenv.2017.03.051

Baklanov, A., Molina, L. T., & Gauss, M. (2016). Megacities, air quality and climate. *Atmospheric Environment*, *126*, 235-249. doi: 10.1016/j.atmosenv.2015.11.059

Bocquet, M., Elbern, H., Eskes, H., Hirtl, M., Žabkar, R., Carmichael, G. R., ... Seigneur, C. (2015, 5). Data assimilation in atmospheric chemistry models: current status and future prospects for coupled chemistry meteorology models. *Atmospheric Chemistry and Physics*, *15*, 5325-5358. doi: 10.5194/acp-15-5325-2015

Brasseur, G. P., & Jacob, D. J. (2017). *Modeling of atmospheric chemistry.* Cambridge University Press.

Brasseur, G. P., Xie, Y., Petersen, A. K., Bouarar, I., Flemming, J., Gauss, M., ... Zhou, G. (2019, 1). Ensemble forecasts of air quality in eastern China-Part 1: Model description and implementation of the MarcoPolo-Panda prediction system, version 1. *Geoscientific Model Development*, *12*, 33–67. doi: 10.5194/gmd-12-33-2019

Carmichael, G. R., Sandu, A., Chai, T., Daescu, D. N., Constantinescu, E. M., & Tang, Y. (2008, 3). Predicting air quality: Improvements through advanced methods to integrate models and measurements. *Journal of Computational Physics*, *227*, 3540-3571. doi: 10.1016/j.jcp.2007.02.024

Carrassi, A., Bocquet, M., Bertino, L., & Evensen, G. (2018, 9). Data assimilation in the geosciences: An overview of methods, issues, and perspectives. *WIREs Climate Change*, *9*. doi: 10.1002/wcc.535

Castell, N., Dauge, F. R., Schneider, P., Vogt, M., Lerner, U., Fishbain, B., ...

Bartonova, A. (2017, 2). Can commercial low-cost sensor platforms contribute to air quality monitoring and exposure estimates? *Environment International*, *99*, 293-302. doi: 10.1016/j.envint.2016.12.007

Cheng, Z., Luo, L., Wang, S., Wang, Y., Sharma, S., Shimadera, H., ... Hao, J. (2016, 4). Status and characteristics of ambient pm2.5 pollution in global megacities. *Environment International*, *89-90*, 212-221. doi: 10.1016/j.envint.2016.02.003

Chin, M., Ginoux, P., Kinne, S., Torres, O., Holben, B. N., Duncan, B. N., ... Nakajima, T. (2002, 2). Tropospheric aerosol optical thickness from the gocart model and comparisons with satellite and sun photometer measurements. *Journal of the Atmospheric Sciences*, *59*, 461-483. doi: 10.1175/1520-0469(2002)059⟨0461:TAOTFT⟩2.0.CO;2

Crippa, M., Solazzo, E., Huang, G., Guizzardi, D., Koffi, E., Muntean, M., ... Janssens-Maenhout, G. (2020, 12). High resolution temporal profiles in the emissions database for global atmospheric research. *Scientific Data*, *7*, 121. doi: 10.1038/s41597-020-0462-2

Deroubaix, A., Brasseur, G., Gaubert, B., Labuhn, I., Menut, L., Siour, G., & Tuccella, P. (2021, 5). Response of surface ozone concentration to emission reduction and meteorology during the covid-19 lockdown in europe. *Meteorological Applications*, *28*. doi: 10.1002/met.1990

Deroubaix, A., Hoelzemann, J. J., Ynoue, R. Y., de Almeida Albuquerque, T. T., Alves, R. C., de Fatima Andrade, M., ... Brasseur, G. (2024, 1). Intercomparison of air quality models in a megacity: Toward an operational ensemble forecasting system for são paulo. *Journal of Geophysical Research: Atmospheres*, *129*. doi: 10.1029/2022JD038179

Doumbia, T., Granier, C., Elguindi, N., Bouarar, I., Darras, S., Brasseur, G., ... Wang, T. (2021, 8). Changes in global air pollutant emissions during the covid-19 pandemic: a dataset for atmospheric modeling. *Earth System Science Data*, *13*, 4191-4206. doi: 10.5194/essd-13-4191-2021

ECMWF. (2023). Copernicus atmosphere monitoring service, [dataset]. *European Center for Medium-Range Weather Forecasts*. Retrieved from `https://ads.atmosphere.copernicus.eu/cdsapp#!/dataset/cams-global-atmospheric-composition-forecasts,[Accessed:08/11/2023]`

Emmons, L. K., Schwantes, R. H., Orlando, J. J., Tyndall, G., Kinnison, D., Lamarque, J. F., ... Pétron, G. (2020, 4). The chemistry mechanism in the community earth system model version 2 (cesm2). *Journal of Advances in Modeling Earth Systems*, *12*. doi: 10.1029/2019MS001882

Emmons, L. K., Walters, S., Hess, P. G., Lamarque, J.-F., Pfister, G. G., Fillmore, D., ... Kloster, S. (2010). Geoscientific model development description and evaluation of the model for ozone and related chemical tracers, version 4 (mozart-4). *Geosci. Model Dev*, *3*, 43-67.

Fast, J. D., Gustafson, W. I., Easter, R. C., Zaveri, R. A., Barnard, J. C., Chapman, E. G., ... Peckham, S. E. (2006, 11). Evolution of ozone, particulates, and aerosol direct radiative forcing in the vicinity of houston using a fully coupled meteorology-chemistry-aerosol model. *Journal of Geophysical Research Atmospheres*, *111*. doi: 10.1029/2005JD006721

Feng, L., Smith, S. J., Braun, C., Crippa, M., Gidden, M. J., Hoesly, R., ... van der Werf, G. R. (2020, 2). The generation of gridded emissions data for cmip6. *Geoscientific Model Development*, *13*, 461-482. doi: 10.5194/gmd-13-461-2020

Freitas, E. D., Rozoff, C. M., Cotton, W. R., & Dias, P. L. S. (2007, 1). Interactions of an urban heat island and sea-breeze circulations during winter over the metropolitan area of são paulo, brazil. *Boundary-Layer Meteorology*, *122*, 43-65. doi: 10.1007/s10546-006-9091-3

Gaubert, B., Bouarar, I., Doumbia, T., Liu, Y., Stavrakou, T., Deroubaix, A., ... Brasseur, G. P. (2021, 4). Global changes in secondary atmospheric pollu-

tants during the 2020 covid-19 pandemic. *Journal of Geophysical Research: Atmospheres*, *126*. doi: 10.1029/2020JD034213

Gettelman, A., Mills, M. J., Kinnison, D. E., Garcia, R. R., Smith, A. K., Marsh, D. R., ... Randel, W. J. (2019, 12). The whole atmosphere community climate model version 6 (waccm6). *Journal of Geophysical Research: Atmospheres*, *124*, 12380-12403. doi: 10.1029/2019JD030943

Giglio, L., Randerson, J. T., & van der Werf, G. R. (2013, 3). Analysis of daily, monthly, and annual burned area using the fourth-generation global fire emissions database (gfed4). *Journal of Geophysical Research: Biogeosciences*, *118*, 317-328. doi: 10.1002/jgrg.20042

Granier, C., Darras, S., van der Gon, H. D., Doubalova, J., Elguindi, N., Galle, B., ... Sindelarova, K. (2019). The copernicus atmosphere monitoring service global and regional emissions (april 2019 version). *Copernicus Atmosphere Monitoring Service*. doi: 10.24380/d0bn-kx16

Grell, Peckham, S. E., Schmitz, R., McKeen, S. A., Frost, G., Skamarock, W. C., & Eder, B. (2005, 12). Fully coupled "online" chemistry within the wrf model. *Atmospheric Environment*, *39*, 6957-6975. doi: 10.1016/j.atmosenv.2005.04.027

Guenther, a., Karl, T., Harley, P., Wiedinmyer, C., Palmer, P. I., & Geron, C. (2006). Estimates of global terrestrial isoprene emissions using MEGAN (Model of Emissions of Gases and Aerosols from Nature). *Atmospheric Chemistry and Physics Discussions*, *6*, 107–173. doi: 10.5194/acpd-6-107-2006

Huang, G., Brook, R., Crippa, M., Janssens-Maenhout, G., Schieberle, C., Dore, C., ... Friedrich, R. (2017, 6). Speciation of anthropogenic emissions of non-methane volatile organic compounds: a global gridded data set for 1970–2012. *Atmospheric Chemistry and Physics*, *17*, 7683-7701. doi: 10.5194/acp-17-7683-2017

Huneeus, N., van der Gon, H. D., Castesana, P., Menares, C., Granier, C., Granier, L., ... Ynoue, R. Y. (2020, 8). Evaluation of anthropogenic air pollutant emission inventories for south america at national and city scale. *Atmospheric Environment*, *235*, 117606. doi: 10.1016/j.atmosenv.2020.117606

Ibarra-Espinosa, S., Ynoue, R. Y., Ropkins, K., Zhang, X., & de Freitas, E. D. (2020, 2). High spatial and temporal resolution vehicular emissions in southeast brazil with traffic data from real-time gps and travel demand models. *Atmospheric Environment*, *222*, 117136. doi: 10.1016/j.atmosenv.2019.117136

Inness, A., Aben, I., Ades, M., Borsdorff, T., Flemming, J., Jones, L., ... Ribas, R. (2022, 11). Assimilation of s5p/tropomi carbon monoxide data with the global cams near-real-time system. *Atmospheric Chemistry and Physics*, *22*, 14355-14376. doi: 10.5194/acp-22-14355-2022

Inness, A., Ades, M., Agusti-Panareda, A., Barré, J., Benedictow, A., Blechschmidt, A.-M., ... Suttie, M. (2019). The CAMS reanalysis of atmospheric composition. *Atmospheric Chemistry and Physics*, *19*(6), 3515-3556. doi: 10.5194/acp-19-3515-2019

Kosmidis, E., Syropoulou, P., Tekes, S., Schneider, P., Spyromitros-Xioufis, E., Riga, M., ... Alexandri, G. (2018, 5). hackair: Towards raising awareness about air quality in europe by developing a collective online platform. *ISPRS International Journal of Geo-Information*, *7*, 187. doi: 10.3390/ijgi7050187

Kumar, P., Morawska, L., Martani, C., Biskos, G., Neophytou, M., Sabatino, S. D., ... Britter, R. (2015, 2). The rise of low-cost sensing for managing air pollution in cities. *Environment International*, *75*, 199-205. doi: 10.1016/j.envint.2014.11.019

Levy, H. (1971, 7). Normal atmosphere: Large radical and formaldehyde concentrations predicted. *Science*, *173*, 141-143. doi: 10.1126/science.173.3992.141

Liang, J., Jackson, B., & Kaduwela, A. (2006, 9). Evaluation of the ability of indicator species ratios to determine the sensitivity of ozone to reduc-

tions in emissions of volatile organic compounds and oxides of nitrogen in northern california. *Atmospheric Environment*, *40*, 5156-5166. doi: 10.1016/j.atmosenv.2006.03.060

Liu, X., Ma, P.-L., Wang, H., Tilmes, S., Singh, B., Easter, R. C., ... Rasch, P. J. (2016). Description and evaluation of a new four-mode version of the modal aerosol module (mam4) within version 5.3 of the community atmosphere model. *Geoscientific Model Development*, *9*(2), 505–522. doi: 10.5194/gmd-9-505-2016

Mailler, S., Khvorostyanov, D., & Menut, L. (2013, 6). Impact of the vertical emission profiles on background gas-phase pollution simulated from the emep emissions over europe. *Atmospheric Chemistry and Physics*, *13*, 5987-5998. doi: 10.5194/acp-13-5987-2013

Monks, P. S., Archibald, A. T., Colette, A., Cooper, O., Coyle, M., Derwent, R., ... Williams, M. L. (2015, 8). Tropospheric ozone and its precursors from the urban to the global scale from air quality to short-lived climate forcer. *Atmospheric Chemistry and Physics*, *15*, 8889-8973. doi: 10.5194/acp-15-8889-2015

NCEP. (2023). ds083.2, [dataset]. *US National Centers for Environmental Prediction*. Retrieved from `https://10.5065/D6M043C6,[Accessed:27/09/2023]` doi: 10.5065/D6M043C6

Nguyen, C. V., & Soulhac, L. (2021, 5). Data assimilation methods for urban air quality at the local scale. *Atmospheric Environment*, *253*, 118366. doi: 10.1016/j.atmosenv.2021.118366

OPENAQ. (2023). Openaq internet platform, [dataset]. *openaq.org*. Retrieved from `https://openaq.org/,[Accessed:04/11/2023]`

Park, H.-S., Kim, R.-E., Park, Y.-M., Hwang, K.-C., Lee, S.-H., Kim, J.-J., ... Choi, W. (2020, 2). The potential of commercial sensors for spatially dense short-term air quality monitoring based on multiple short-term evaluations of 30 sensor nodes in urban areas in korea. *Aerosol and Air Quality Research*, *20*, 369-380. doi: 10.4209/aaqr.2019.03.0143

Petersen, A. K., Brasseur, G. P., Bouarar, I., Flemming, J., Gauss, M., Jiang, F., ... Zhou, G. (2019, 4). Ensemble forecasts of air quality in eastern china-part 2: Evaluation of the marcopolo-panda prediction system, version 1. *Geoscientific Model Development*, *12*. doi: 10.5194/gmd-12-1241-2019

Pfister, G. G., Avise, J., Wiedinmyer, C., Edwards, D. P., Emmons, L. K., Diskin, G. D., ... Wisthaler, A. (2011, 8). Co source contribution analysis for california during arctas-carb. *Atmospheric Chemistry and Physics*, *11*, 7515-7532. doi: 10.5194/acp-11-7515-2011

Powers, J. G., Klemp, J. B., Skamarock, W. C., Davis, C. A., Dudhia, J., Gill, D. O., ... Duda, M. G. (2017). The weather research and forecasting model: Overview, system efforts, and future directions. *Bulletin of the American Meteorological Society*, *98*(8), 1717-1737. doi: 10.1175/BAMS-D-15-00308.1

Rémy, S., Kipling, Z., Flemming, J., Boucher, O., Nabat, P., Michou, M., ... Morcrette, J.-J. (2019, 11). Description and evaluation of the tropospheric aerosol scheme in the european centre for medium-range weather forecasts (ecmwf) integrated forecasting system (ifs-aer, cycle 45r1). *Geoscientific Model Development*, *12*, 4627-4659. doi: 10.5194/gmd-12-4627-2019

Sokhi, R. S., Moussiopoulos, N., Baklanov, A., Bartzis, J., Coll, I., Finardi, S., ... Kukkonen, J. (2022, 4). Advances in air quality research – current and emerging challenges. *Atmospheric Chemistry and Physics*, *22*, 4615-4703. doi: 10.5194/acp-22-4615-2022

Theloke, J., & Friedrich, R. (2007, 6). Compilation of a database on the composition of anthropogenic voc emissions for atmospheric modeling in europe. *Atmospheric Environment*, *41*, 4148-4160. doi: 10.1016/j.atmosenv.2006.12.026

Venter, Z. S., Aunan, K., Chowdhury, S., & Lelieveld, J. (2020, 8). Covid-19 lock-

downs cause global air pollution declines. *Proceedings of the National Academy of Sciences*, *117*, 18984-18990. doi: 10.1073/pnas.2006853117

Viaene, P., Belis, C., Blond, N., Bouland, C., Juda-Rezler, K., Karvosenoja, N., ... Volta, M. (2016, 11). Air quality integrated assessment modelling in the context of eu policy: A way forward. *Environmental Science & Policy*, *65*, 22-28. doi: 10.1016/j.envsci.2016.05.024

Vivanco, M. G., & de Fatima Andrade, M. (2008). Relation between ozone levels and nox and voc emissions in the sao paulo metropolitan area for an episode of august, 1998. *International Journal of Environment and Pollution*, *35*, 90. doi: 10.1504/IJEP.2008.021133

Wesseling, Ruiter, Blokhuis, Drukker, Weijers, Volten, ... Tielemans (2019, 8). Development and implementation of a platform for public information on air quality, sensor measurements, and citizen science. *Atmosphere*, *10*, 445. doi: 10.3390/atmos10080445

Wiedinmyer, C., Akagi, S. K., Yokelson, R. J., Emmons, L. K., Al-Saadi, J. A., Orlando, J. J., & Soja, A. J. (2011, 7). The fire inventory from ncar (finn): a high resolution global model to estimate the emissions from open burning. *Geoscientific Model Development*, *4*, 625-641. doi: 10.5194/gmd-4-625-2011

Zhang, Y., Wen, X., Wang, K., Vijayaraghavan, K., & Jacobson, M. Z. (2009, 11). Probing into regional o3 and particulate matter pollution in the united states: 2. an examination of formation mechanisms through a process analysis technique and sensitivity study. *Journal of Geophysical Research: Atmospheres*, *114*. doi: 10.1029/2009JD011900

Appendix A Supplemental Tables and Figures (see separate document)

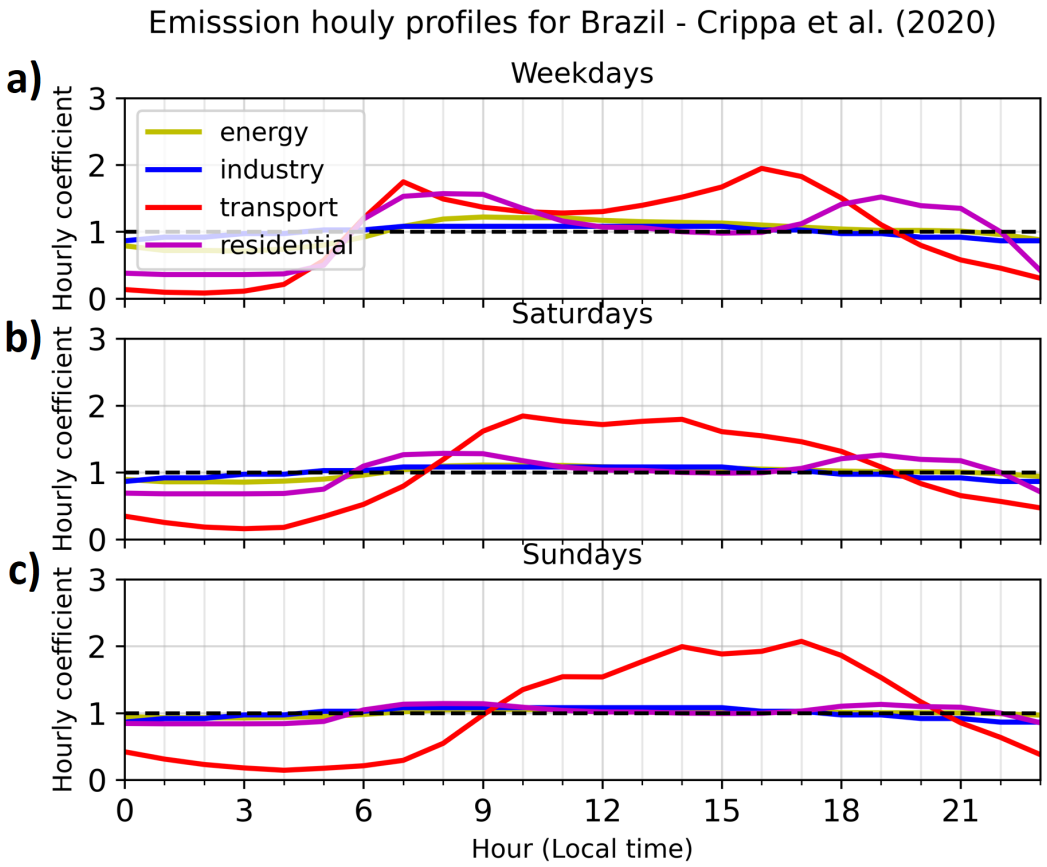

Figure A1. *Sectoral hourly profiles of anthropogenic emission for Brazil proposed by Crippa et al. (2020).*

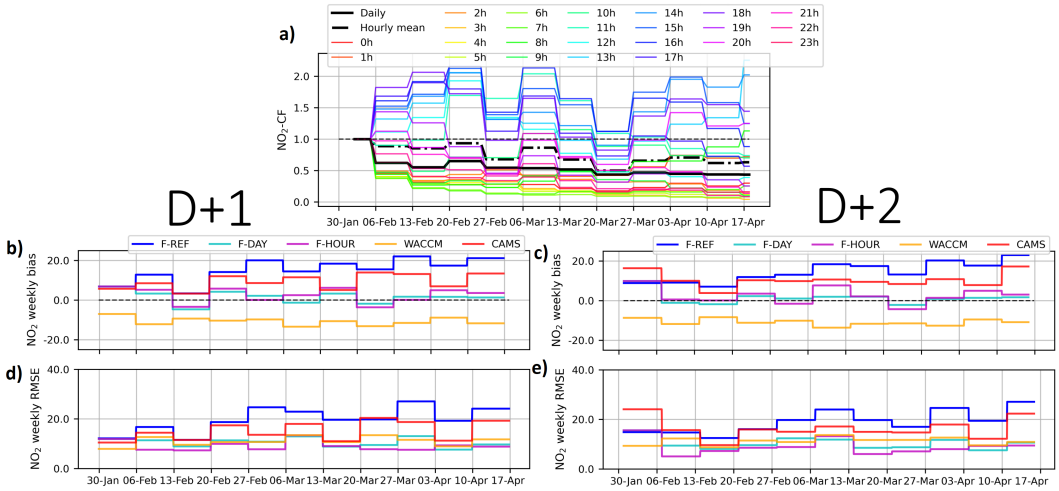

Figure A2. *(a) Weekly evolution of daily and hourly NO_2 correction factors (CF) used for the daily and hourly emission-scaled forecasts (F-DAY and F-HOUR) of a given week. Hours are given in local time (GMT-3). (b, c, d and e) Comparison of the weekly statistical performance (mean bias and RMSE) for NO_2 concentration (in ppb) of the forecasts for the next day (d+1) and the day after (d+2) over the 10-week period (in 2023) in the center of São Paulo, for the three regional forecasts (F-REF, F-DAY and F-HOUR), and for the two global forecasts: (iv) WACCM provided by NCAR and (v) CAMS provided by ECMWF, over the 10-week period (in 2023) in the center of São Paulo.*

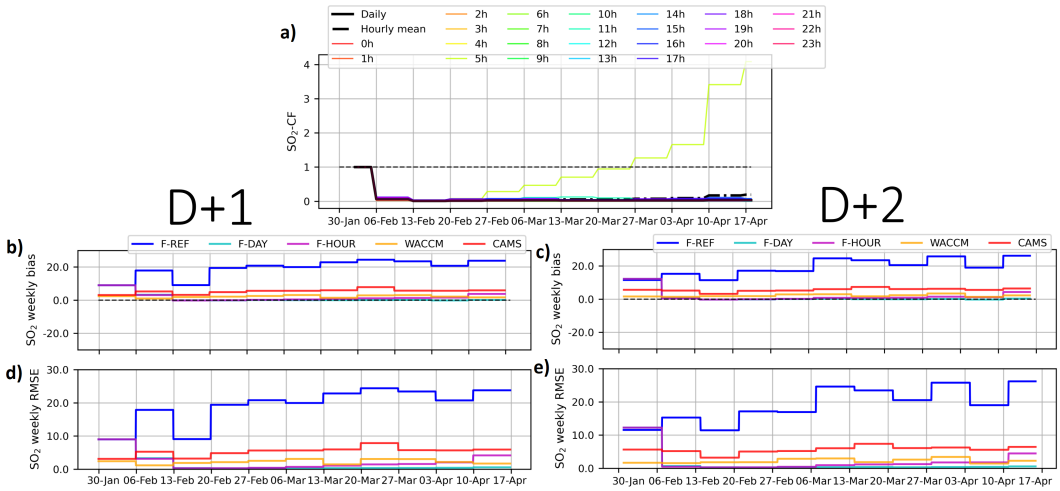

Figure A3. *(a) Weekly evolution of daily and hourly SO_2 correction factors (CF) used for the daily and hourly emission-scaled forecasts (F-DAY and F-HOUR) of a given week. Hours are given in local time (GMT-3). (b, c, d and e) Comparison of the weekly statistical performance (mean bias and RMSE) for SO_2 concentration (in ppb) of the forecasts for the next day (d+1) and the day after (d+2) over the 10-week period (in 2023) in the center of São Paulo, for the three regional forecasts (F-REF, F-DAY and F-HOUR), and for the two global forecasts: (iv) WACCM provided by NCAR and (v) CAMS provided by ECMWF, over the 10-week period (in 2023) in the center of São Paulo.*

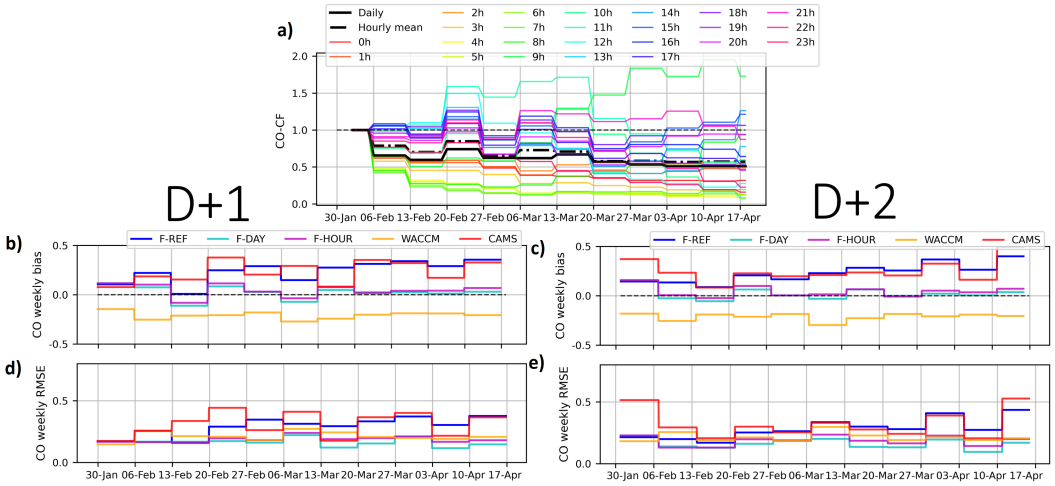

Figure A4. *(a) Weekly evolution of daily and hourly CO correction factors (CF) used for the daily and hourly emission-scaled forecasts (F-DAY and F-HOUR) of a given week. Hours are given in local time (GMT-3). (b, c, d and e) Comparison of the weekly statistical performance (mean bias and RMSE) for CO concentration (in ppm) of the forecasts for the next day (d+1) and the day after (d+2) over the 10-week period (in 2023) in the center of São Paulo, for the three regional forecasts (F-REF, F-DAY and F-HOUR), and for the two global forecasts: (iv) WACCM provided by NCAR and (v) CAMS provided by ECMWF, over the 10-week period (in 2023) in the center of São Paulo.*

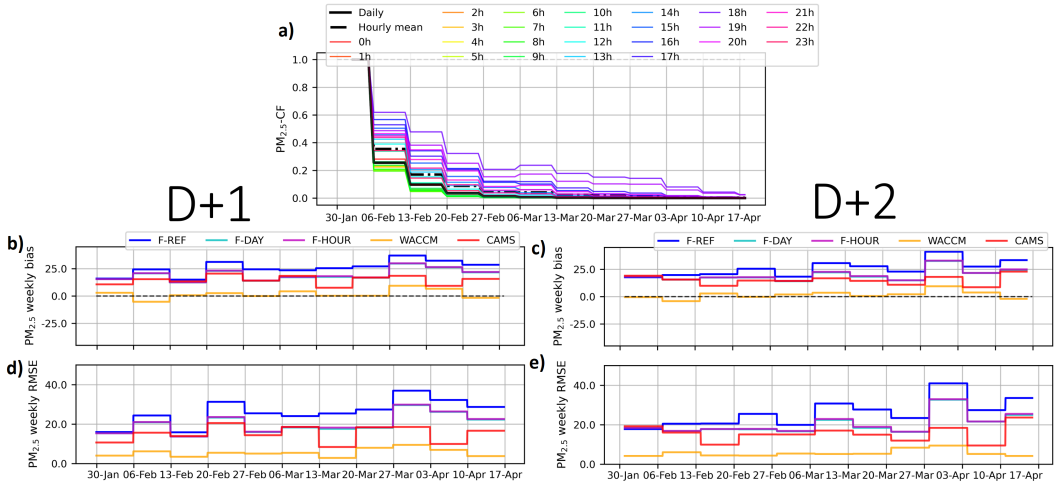

Figure A5. *(a) Weekly evolution of daily and hourly $PM_{2.5}$ correction factors (CF) used for the daily and hourly emission-scaled forecasts (F-DAY and F-HOUR) of a given week. Hours are given in local time (GMT-3). (b, c, d and e) Comparison of the weekly statistical performance (mean bias and RMSE) for $PM_{2.5}$ concentration (in $\mu g.m^{-3}$) of the forecasts for the next day (d+1) and the day after (d+2) over the 10-week period (in 2023) in the center of São Paulo, for the three regional forecasts (F-REF, F-DAY and F-HOUR), and for the two global forecasts: (iv) WACCM provided by NCAR and (v) CAMS provided by ECMWF, over the 10-week period (in 2023) in the center of São Paulo.*

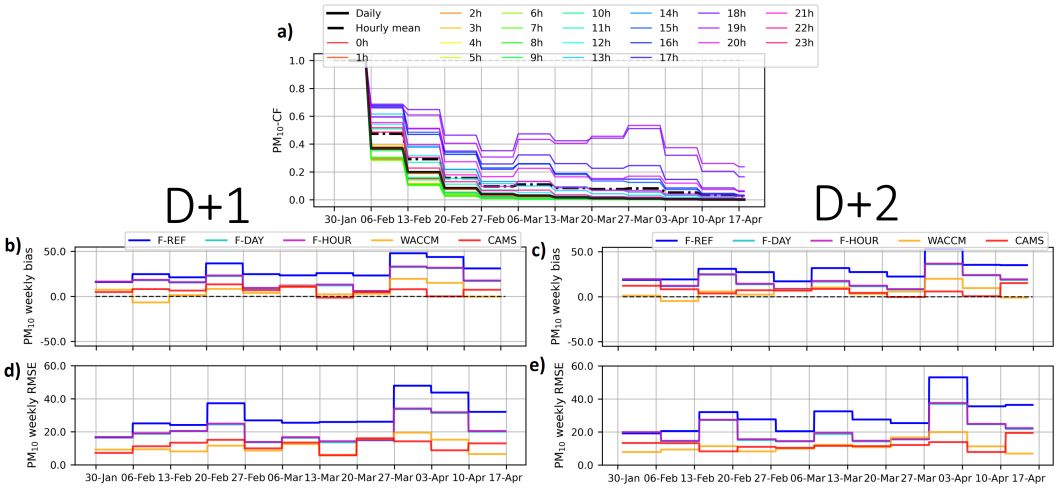

Figure A6. *(a) Weekly evolution of daily and hourly PM_{10} correction factors (CF) used for the daily and hourly emission-scaled forecasts (F-DAY and F-HOUR) of a given week. Hours are given in local time (GMT-3). (b, c, d and e) Comparison of the weekly statistical performance (mean bias and RMSE) for PM_{10} concentration (in $\mu g.m^{-3}$) of the forecasts for the next day (d+1) and the day after (d+2) over the 10-week period (in 2023) in the center of São Paulo, for the three regional forecasts (F-REF, F-DAY and F-HOUR), and for the two global forecasts: (iv) WACCM provided by NCAR and (v) CAMS provided by ECMWF, over the 10-week period (in 2023) in the center of São Paulo.*

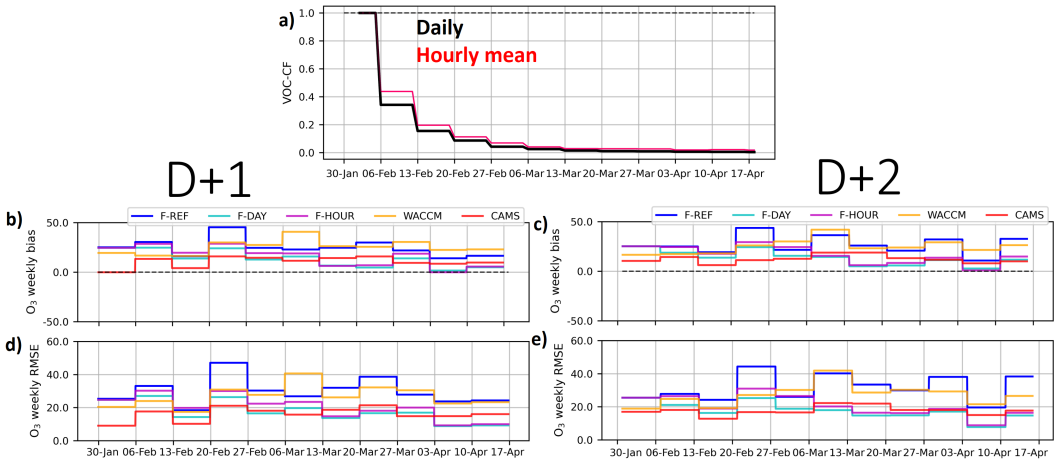

Figure A7. *(a) Weekly evolution of daily and hourly O_3 correction factors (CF) used for the daily and hourly emission-scaled forecasts (F-DAY and F-HOUR) of a given week. Hours are given in local time (GMT-3). (b, c, d and e) Comparison of the weekly statistical performance (mean bias and RMSE) for NO_2 of the forecasts for the next day (d+1) and the day after (d+2) over the 10-week period (in 2023) in the center of São Paulo, for the three regional forecasts (F-REF, F-DAY and F-HOUR), and for the two global forecasts: (iv) WACCM provided by NCAR and (v) CAMS provided by ECMWF, over the 10-week period (in 2023) in the center of São Paulo.*

Table A1. *Configurations of the air quality models for which the forecasts are analyzed: the WACCM forecast (provided by NCAR), the CAMS forecast (provided by ECMWF) and the regional forecasts made with the WRFchem model.*

Forecast	WACCM	CAMS	F-REF, F-DAY, F-HOUR
Institution	NCAR	ECMWF	MPI-IUP
Model	CESM2	IFS	WRFchem (version 4.3.3)
		Domain	
Horizontal resolution	0.95° × 1.25°	40 km	10 km
Domain extension	Global	Global	regional (80 x 80 grid cells)
Vertical levels	70	137	37
Output frequency	6h	3h	1h
		Emission	
Anthropogenic	CMIP6 (Feng et al., 2020)	CAMS-GLOB-ANTv5.3 (Granier et al., 2019)	CAMS-GLOB-ANTv4.2 (Granier et al., 2019)
Anthr. temporal profiles	None	CAMS-GLOB-ANTv5.3	(Crippa et al., 2020)
Anthr. vertical profiles	None	CAMS-GLOB-ANTv5.3	(Mailler et al., 2013)
Biogenic	MEGANv2.1 (Guenther et al., 2006)	MEGANv2.1 (Guenther et al., 2006)	MEGANv2.1 (Guenther et al., 2006)
Fires	GFED4 (Giglio et al., 2013)	CAMS-GFASv1.4 (Inness et al., 2022)	FINNv1 (NRT) (Wiedinmyer et al., 2011)
		Gas and aerosol	
Chemical mechanism	MOZART4-T1 (Emmons et al., 2020)	CB05 (Inness et al., 2019)	MOZART4 (Emmons et al., 2010)
Aerosol scheme	MAM4 (Liu et al., 2016)	IFS-AER (Rémy et al., 2019)	GOCART (Chin et al., 2002)
Boundary conditions	None	None	WACCM